17th Brazilian Congress of Thermal Sciences and Engineering
November 25th-28th, 2018, Águas de Lindóia, SP, Brazil

ENCIT-2018-XXXX
EXPERIMENTAL CHARACTERIZATION ANNULAR IMPINGING JETS

Luiz Fernando Bermero Nardi, lfbnardi@gmail.com

Igor Braga de Paula, igordepaula@puc-rio.br

PUC-RIO - Departamento de Engenharia Mecânica,
Rua Marques de São Vicente, 225, Gávea, Rio de Janeiro-RJ, 22451-000

Abstract. *This study characterizes an impinging jet confined in the annular space between two concentric circular pipes. This geometry is commonly found in most gas injection wells. The experiments were carried out in a test bench, built with transparent pipes. Thus, optical measurement techniques could be adopted. Measurements were divided into velocimetry and heat transfer tests. For the velocity measurements, time resolved Particle Image Velocimetry techniques were employed. A planar configuration was chosen, hence only measurements in plane with the jet are presented. A set of 49 experiments with different configurations with respect to the number of jets within the annular space, the Reynolds number and the radial distance of the annular space are presented. Results show that confined impinging jet exhibits similarities with the case of an impinging jet of a flat surface. The flow fluctuations were analyzed in the frequency domain and most dominant structures were extracted from Proper Orthogonal Decomposition of the velocity flow field. For heat transfer experiments, a thermal camera was employed to acquire the temperature distribution around the pipe with a heated surface. The results were compared against correlations for Nusselt numbers available in the literature.*

Keywords: *Flow-induced-vibration, Impinging jet, Annular flow, PIV, Particle image velocimetry, POD*

1. INTRODUCTION

Flow-induced vibrations have been showing growing importance for oil industry, due to the high Reynolds numbers found inside wellbores. Even though harmless to most of the well hardware, long-term exposure to pressure fluctuations related with flow turbulence can weaken some components of the production string, especially the lines of hydraulic controls.

The flow field of an impinging jet confined in the annular space between two concentric pipes is not known yet. This geometry is, indeed, rather specific and unprecedented in academic literature. Therefore, it was decided to present a review for the closest scenario which correspond to a impinging jet on concave surface.

Impinging jets are widely applied, in industry. They can considerably increase rates of heat and mass transfer on a surface. Some examples include cooling of electronic circuits, combustion chambers and high-ovens.

Jets can also be found at the energy industry, in injection wells of water or gas. High inflow rates are blasted against wellbore walls, through tiny orifices of flow control devices. During this injection, complications can arise from occasional flow-induced vibrations.

On the oil and gas industry, high Reynolds number are present, even to the order of 10^6, which are very difficult to reproduce in a wind tunnel. Impinging jets can be divided into four zones: turbulent free layer, curved vortex wake, stagnation region and, finally, a wall profile. A potential core can also be defined, as the region where flow speed falls until 95% of its upstream value.

In 1999, Cornaro et al. was able to visualize an impinging jet blowing against both concave and convex surfaces, using smoke visualization techniques, for high values of curvature (up to d/D = 0.38). He showed that, if the distance between nozzle and surface falls below the potential core length, coherent vortexes are generated on to the curved surfaces. However, for larger distances, as well as some critical values of L/D, a strong oscilations of the stagnation point were observed. L/D is the non-dimensional distance between jet and plate, while d/D is the ratio between plate curvature diameter and nozzle diameter.

Another important contribution in velocimetry these jets was made by Hashiebaf, in 2015. He measured an impinging jet over concave surface. Several velocity profiles were obtained and found to be very similar to a free-jet, except for a sudden velocity drop near the wall. A very interesting result of the latter study was the capturing of the notable turbulent structures around the jet.

Even though flow inside pipes have been extensively studied throughout literature, little has been produced for annular flows, especially considering turbulence and vibration phenomena. This study aims to investigate the vortex formed by an annular impinging jet and the implication of such vortexes on vibration of structures. The method chosen

for velocity measurements is the well-established Particle Image Velocimetry (PIV), followed by Proper Orthogonal Decomposition (POD) of the velocity fields. This last technique was employed for identification of dominant structures in turbulent flow.

Concerning the heat transfer analyses, important contributions were made by Choi (2001) and Kayansayan (2001), who observed the occurrence of a sencondary peak in the Nusselt number distribution, probably associated with the greater turbulence present in this region, in reference to the stagnation point. Gori (2000) were able to obtain numerical correlations to the Nusselt number for an impinging jet on a cylinder. Chauchat (2016) has made contributions for heat transfer in a confined annular space,.a geometry similar to ours. He, however, employed inward impinging jets.

2. METHODOLOGY

2.1 Experimental set-up

The test rig built for current experiments is shown schematically in Figure 1. It consists of a centrifugal pump, a flowmeter, transparent plexiglass pipes, a visualization box, a laser, a chiller and a camera. The working fluid was is filtered water. The rig worked in a closed loop, therefore the water temperature increased with time due to heat transfer with the pump. In order to stabilize the water temperature a chiller Huber K12 was used to control the temperature within ±0.5ºC during the experiments. The fluid temperature was monitored with a Pt-100 sensor. The laser beam was conditioned with cylindrical and spherical lenses to form an illumination plan for Particle Image Velocimetry (PIV) measurements. Silver coated hollow glass spheres with 20um of diameter were used as tracers. The illumination was provided by high speed laser manufactured by LITRON (model LDY304). It has a double cavity and it is capable to provide 30mJ/pulse of illumination at a frequency of 1KHz. Therefore, time resolved PIV measurements were performed. A high speed camera (IDT Motion Pro X3) with resolution of 2MPx was used. The laser and the camera were synchronized with a BNC575 synchronizer. In the current experiments, images pair for PIV analysis were acquired at a rate of 400 frames per second.

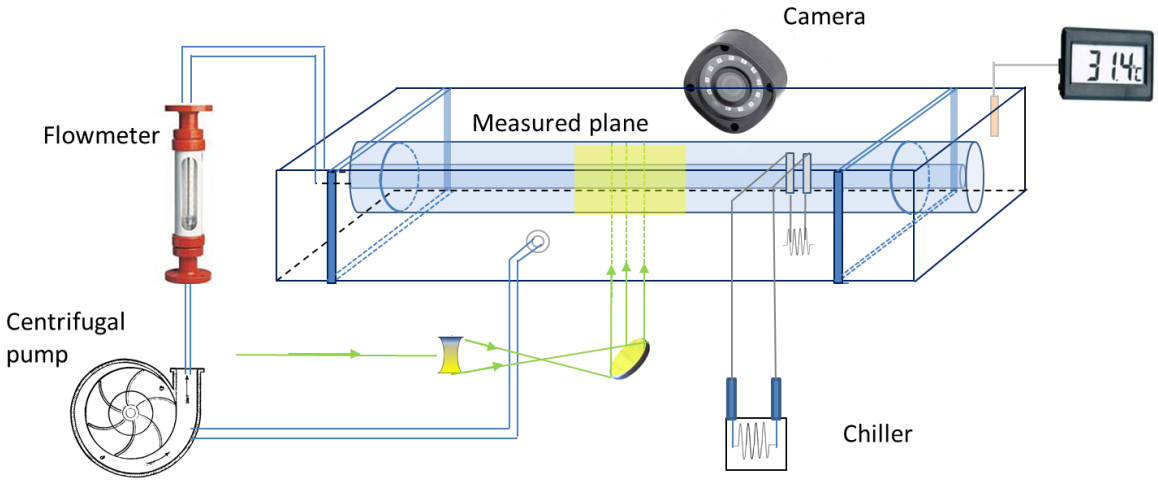

Figure 1 – Experimental set-up for the PIV

Figure 2 shows some of the configurations investigated in this work. According to the figure, water is injected in the inner pipe and then ejected through small holes oriented normal to the outer pipe surface. The idea is to observe how multiple jets can modify the flow when compared to the case of a single jet. In case of multiple jets an interaction might occur and the jet can exhibit a strong oscillation.

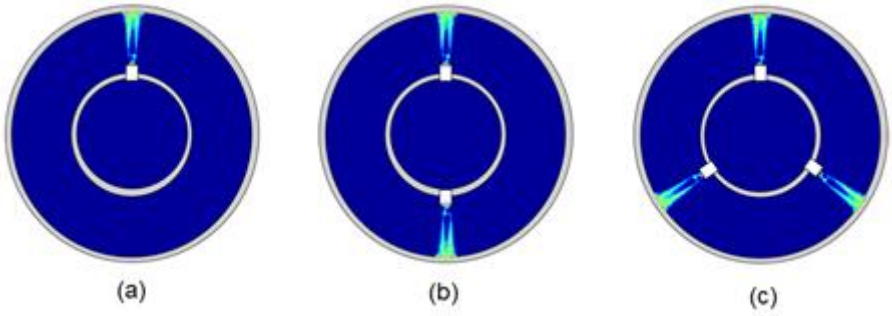

Figure 2 – Different types of cross-section used for flow injection.

For planar impinging jets, one of the most important parameters is the non-dimensional distance between jet and plate (L/d). In the annular configuration, distance between jet and surface varied by changing the diameters of inner and outer pipes, while keeping them concentric. We denote by L the radial distance between inner and outer cylinders, that is, equals to $\frac{(ID\ outer\ tube - OD\ inner\ tube)}{2}$.

For each geometric combination, three different values of flow rate were used, so that the effect of the Reynolds number ($Re_d = \frac{U_0\, d}{\upsilon}$) could be observed, where υ is the dynamic viscosity, d is the jet diameter ($d = 6{,}35mm$) and U_0 is the mean velocity at the orifice exit. Different combinations of pipe geometries and flow rates were considered. In this paper only a few are presented

The PIV fields were processed using the Multi-Pass-Hart algorithm. A set of PIV routines written in Matlab were used for data processing. Interrogation windows of 16x16 pixels were used with an overlap of 75%. Thereby, the resolution was rather refined in the annular space. This was important for characterization of the jet structure. More details about this and other available PIV Process Methods can be found in Abrantes et al. [1].

One of challenges in the present work was the determination of dominant frequencies of flow fluctuation. To this end, standard FFT algorithms were employed to transform the time resolved flow fields into frequency domain. Afterwards, dominant frequencies in the Fourier spectra were spatially analyzed using Proper Orthogonal Decomposition. Thus, the spatial structures related with most energetic fluctuations could be recovered. The snapshot POD technique is used following the work of Berkooz et al (1993).

Heat transfer measurements were also. To this end, a portion of the outer cylinder wall was cut out and replaced with an electric film, as shown in Figure 3.

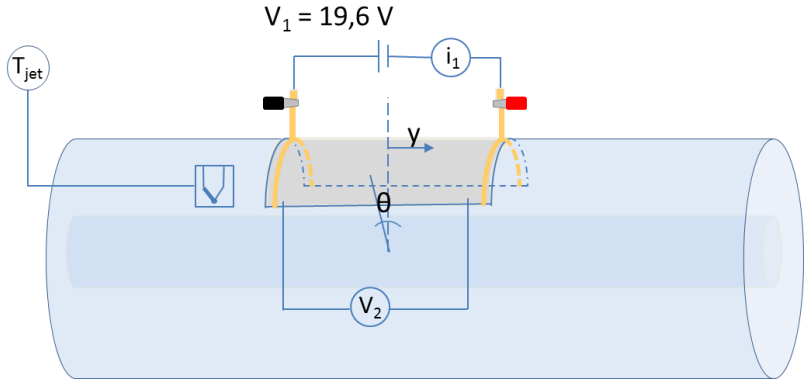

Figure 3 – Heated plate installed on outer cylinder

A controlled current was be applied to the film, in order to adjust the heat generated at the surface. The surface temperature was measured with an infrared thermal camera, whereas the average temperature of the impinging jet, T_{jet}, was measured with a thermocouple, placed in the annular space between cylinders. The Nusselt number distribution was calculated, for several geometries and flow rates, by applying

$$Nu_d\,(y,\theta) = \frac{h\,(y,\theta)\,\cdot\,d}{k_w} = \frac{\ddot{q}}{\left[T(y,\theta) - T_{jet}\right]}\,\cdot\frac{d}{k_w} \qquad (2.1)$$

Nu_d is the local Nusselt number, at point (y, θ), according to the coordinate system indicated in Figure 2. h is the local convection coefficient, $T(y, \theta)$ the local temperature, obtained through thermal imaging. d is the nozzle diameter, worth 6.35 mm for all experiments. k_w is the water conductivity, taken as $k_w = 0.591 \frac{W}{m\,K}$.

To calculate the heat transfer per area, $\ddot{q}$, it was necessary to measure the voltage V_2, across the film, as well as the current established throughout the circuit, i_1. Since this was a continuous current, $\ddot{q} = \frac{V_2\ i_1}{S_{plate}}$.

S_{plate} is the heated surface of the plate given by $S_{plate} = \frac{120°}{360°} \cdot \pi \frac{OD^2}{4} = 2{,}513.3\ mm^2$. Substituting these values into Eq. (2.1), we obtain:

$$Nu_d\ (y, \theta) = \frac{V_2\ i_1}{S_{plate} \cdot [T(y, \theta) - T_{jet}]} \cdot \frac{d}{k_w} \qquad (2.2)$$

To obtain $T(y, \theta)$, a series of thermal images were obtained with a FLIR® E4 infrared camera, with resolution of 4,800 pixels. For each case, it was necessary to photograph 50 images of the plate, without heating, and another 50 images with heating. The image sets were averaged, to eliminate instantaneous oscillations found in the thermal fields.

3. RESULTS

Figure 4 shows the measured fluctuations in axial velocity, u, for the configuration with 2 jets in cross-section, as showed in Figure 2(b).

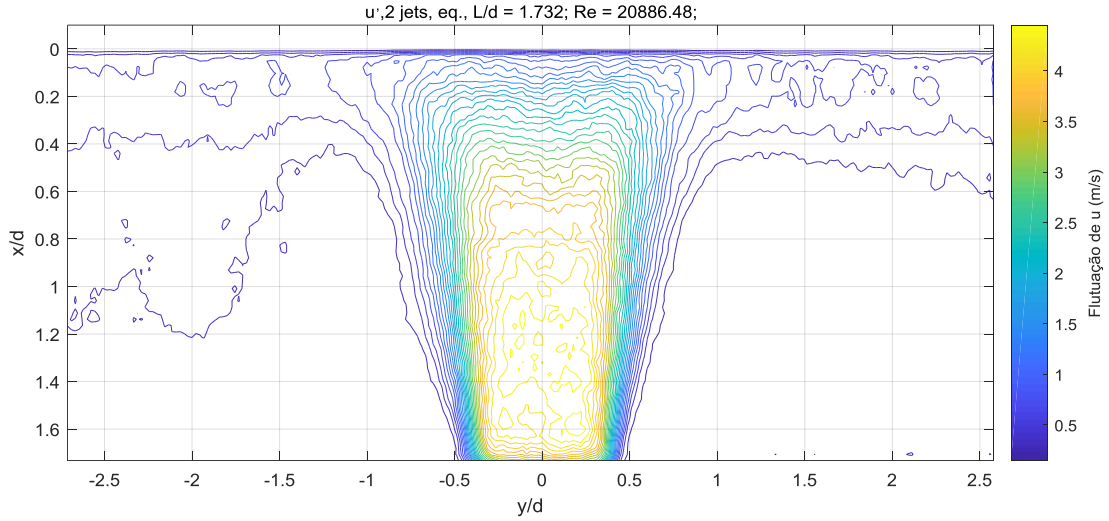

Figure 4 – Contours of u', 2 jets on cross-section; L/d = 1.7323; Re = 20,886.48;

Figure 5 shows contours of crosswise velocity fluctuation, for the same configuration.

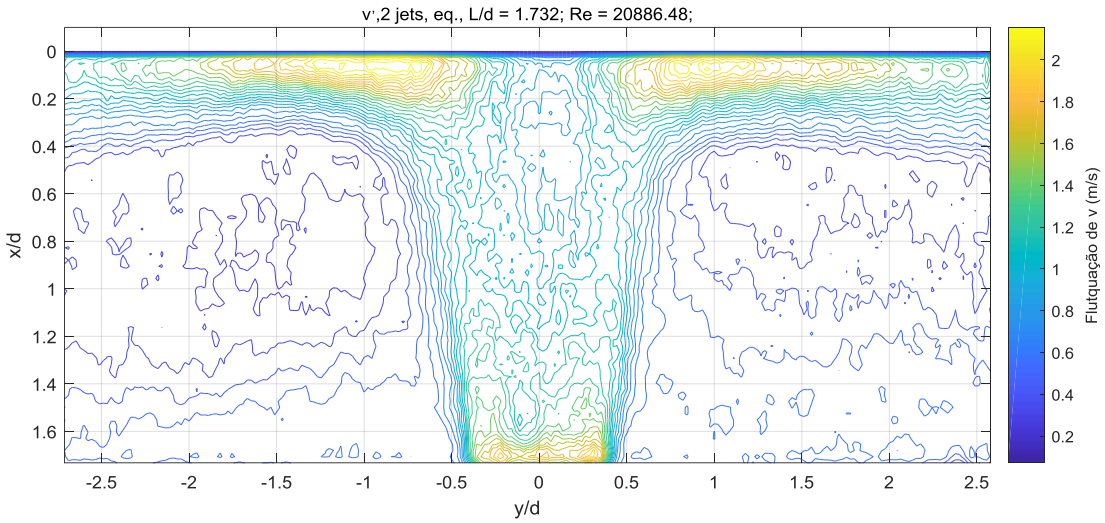

Figure 5 – Contours of v', 2 jets on cross-section; L/d = 1.7323; Re = 20,886.48

These results are well in line with most non-confined impinging jets. One can notice that higher turbulence is located at the edges of the jet, due to the mixing layer. At the wall, the flow is mixed and the turbulence exhibits higher fluctuation on component v, parallel to the pipe axis.

All literature for free jet points out that $\frac{x}{d} \in [0\,;4]$ represents the region where the issuing speed of the jet remains unaffected. This region is the so-called potential core of the jet. No potential core was observed in the present work, since all $\frac{L}{d}$ distances were chosen below $\frac{L}{d} = 2$.

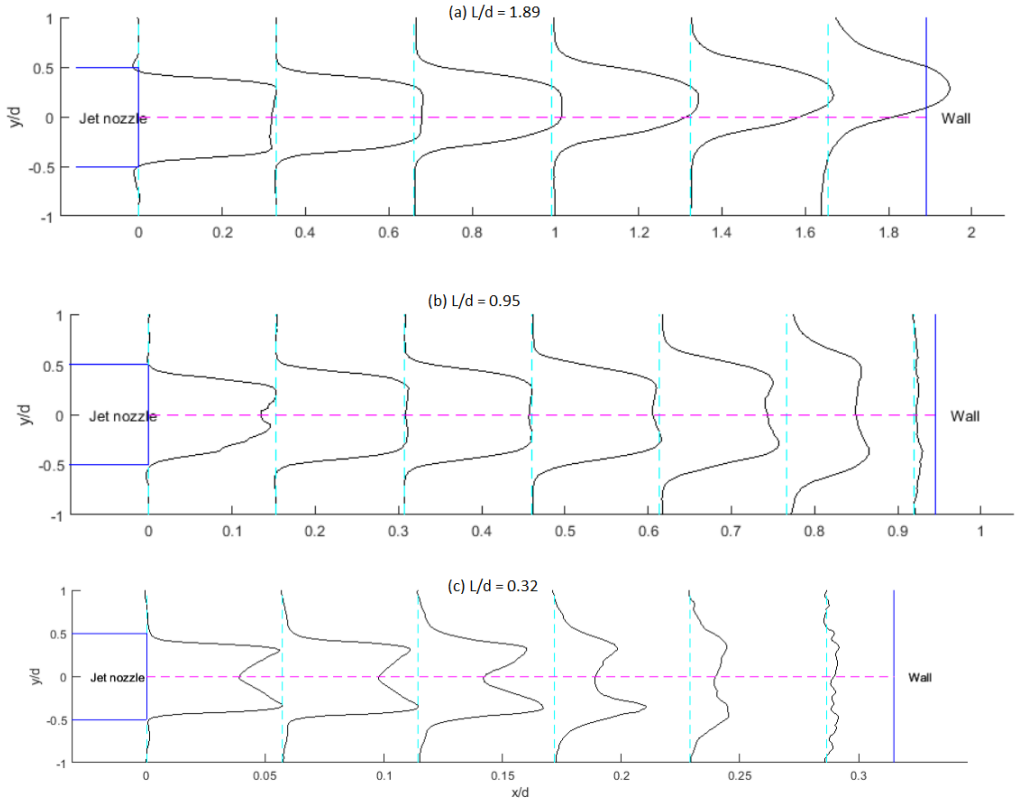

Figure 6 – u_{med} profiles, 1 jet, Re = 13,924

As the distance between jet and plate was decreased, the jet entrainment effect became more pronounced in the inner portion of the jet, causing u_{med} profiles to vary from convex to concave shape, as shown in Figure 6.

Figure 7 shows an interesting result, for the streamwise velocity in the centerline of the jets. While, for free jets, the core velocity monotonically decreases with x, for the annular jet, a different behavior occurs. As the observer moves away from the nozzle, the flow is found to accelerate, up to a maximum value, and then decelerate, until $u_{med} = 0$, at the stagnation point.

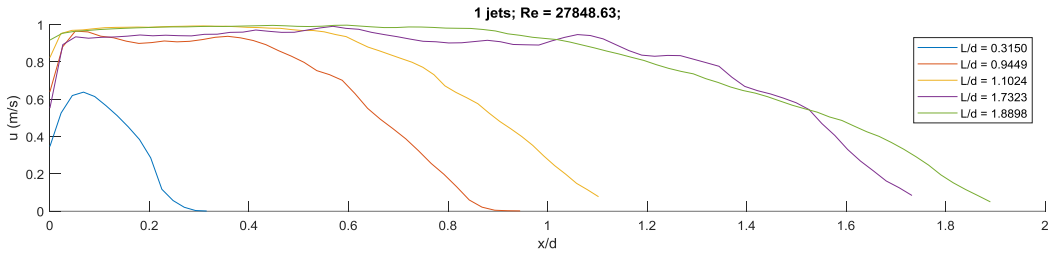

Figure 7 –Evolution of u_{med} on centerline, for the highest Reynolds number employed

The streamwise evolution of r.m.s fluctuations of the streamwise speed is well in line with results from (A. Hashiehbaf, 2015), with u'_{rms} reaching values in the order of 10% of the jet exit speed.

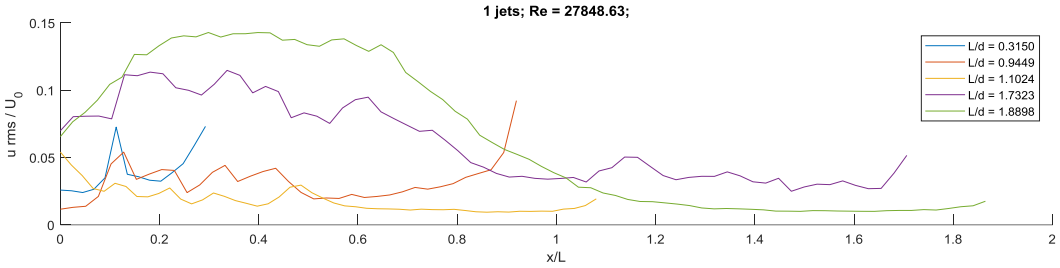

Figure 8 – Evolution of u'_{rms} on centerline, for Re = 27,848

In the present work, u'_{rms} has a sudden increase, near the impingement wall, for all geometries observed. This differs from Hasheibaf's observations, since all his u'_{rms} had a sudden decrease, near wall.

Velocity fluctuations, as expected, increase at increasing Reynolds numbers, as shown in Figure 9.

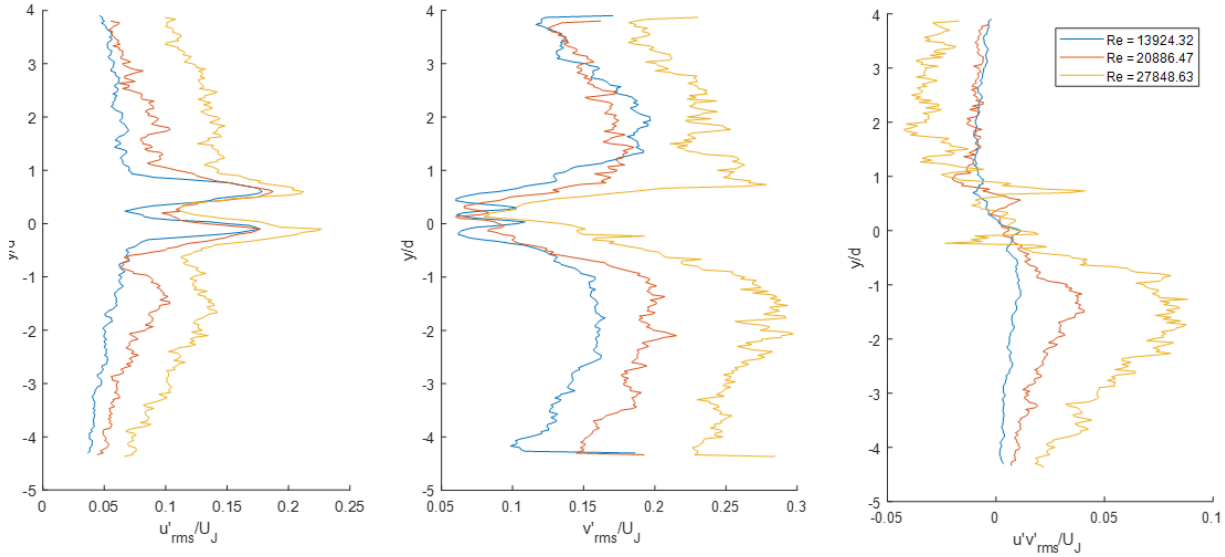

Figure 9 – Velocity fluctuations at $\frac{x}{L} = 0.9$, for 1 jet ; $\frac{L}{d} = 1.7323$

For the lowest Reynolds number studied, $Re = 13{,}924$, it was uncovered that, as the number of jets per section increases, fluctuations u'_{rms} and v'_{rms} also increase, at $\frac{x}{L} = 0.9$. The correlation $u'v'_{rms}$, however, had a unique behavior, as shown in Figure 7. It was found to assume negative values in approximately half of the domain, as opposed to what was discovered by (Maurell & Solliec, 2001). This author, who analyzed jets impinging over a flat surface, discovered that a region occurred, near the stagnation point, where $u'v'_{rms}$ was negative in 13% of the domain.

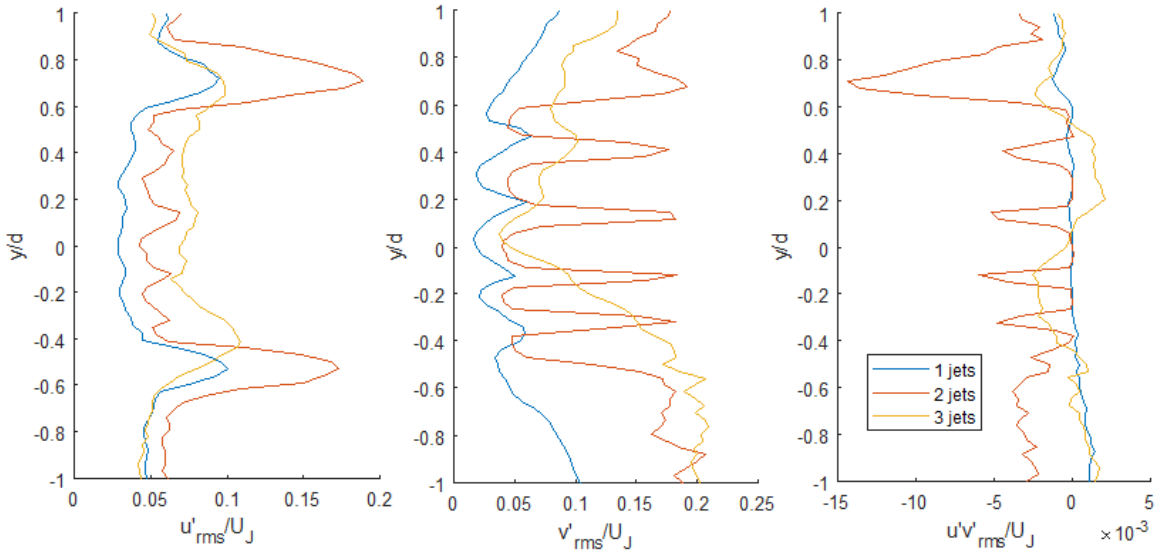

Figure 10 – Velocity fluctuations at $\frac{x}{L} = 0.9$, for $\frac{L}{d} = 1.1024$; $Re = 13{,}924$

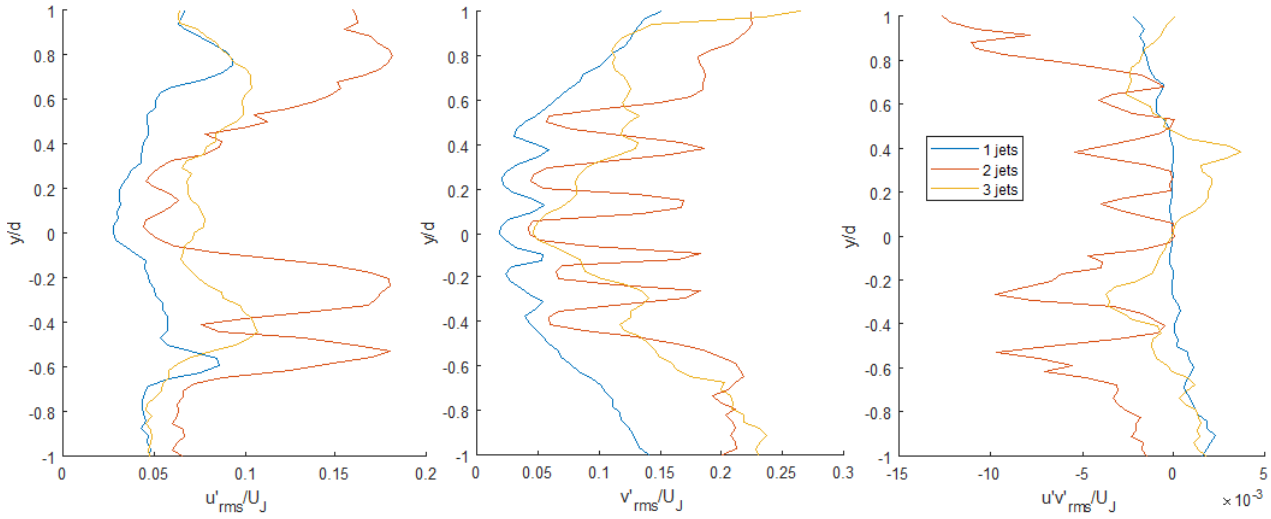

Figure 11 – Velocity fluctuations at $\frac{x}{L} = 0.9$, for $\frac{L}{d} = 1.1024$; $Re = 20{,}886$

These results were replicated for $Re = 20{,}886$. A strong spatial oscillation was observed for the Reynolds tensions, especially for v'_{rms}, which presented consistent peaks, separated by a period of $\lambda_{v'} = 0.2\,d$. This indicates the that coherent vortices could be forming at the wall region, especially for the 2 jets geometry.

For the highest Reynolds number analyzed, $Re = 27{,}848$, fluctuations are shown in Figure 12.

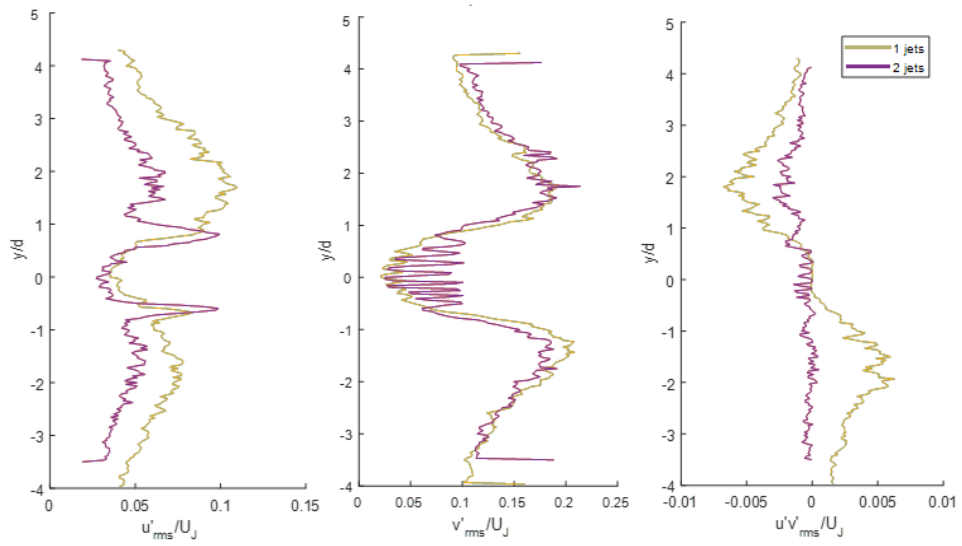

Figure 12 – Velocity fluctuations at $\frac{x}{L} = 0.9$, for $\frac{L}{d} = 1.1024$; $Re = 27{,}848$

For $Re = 27{,}848$, the 2-jet-geometry appears to stabilize the flow, producing less fluctuations than the single jet configuration.

An attempt was made to search for distinguished frequencies within the oscillations observed in both u and v signals. Therefore, a modal analysis of the velocity signals was performed. For this analysis, the domain was restricted to the jet borders, where the Kelvin-Helmholz instability occurs, and to the region near wall where high velocity fluctuations were encountered.

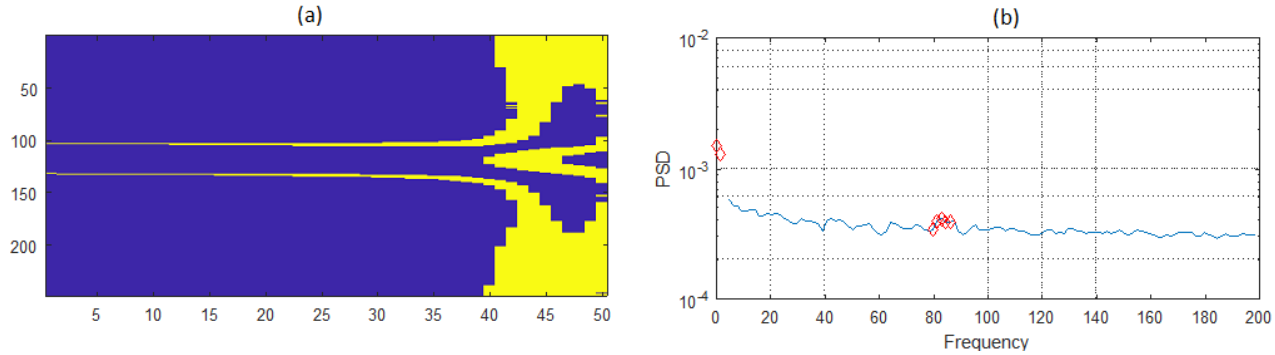

Figure 13 – Case 7; 1 jet ; $\frac{L}{d} = 1.1024$; $Re = 13{,}924$ (a) Sub-domain for modal analysis (b) Power Spectrum Density of v'_{rms}

The PSD counted the dominant frequencies in the power spectrum density of the velocity signals. As no frequency stood out, for most of the analyzed cases, an attempt was made to perform the Proper Orthogonal Decomposition (POD) based on frequency bands, rather than discrete frequency values. The POD utilized 1 thousand snapshots of u and v speeds and yielded 20 orthogonal modes for the signal reproduction. Figure 14 shows the 4 main modes encountered for case nº 7.

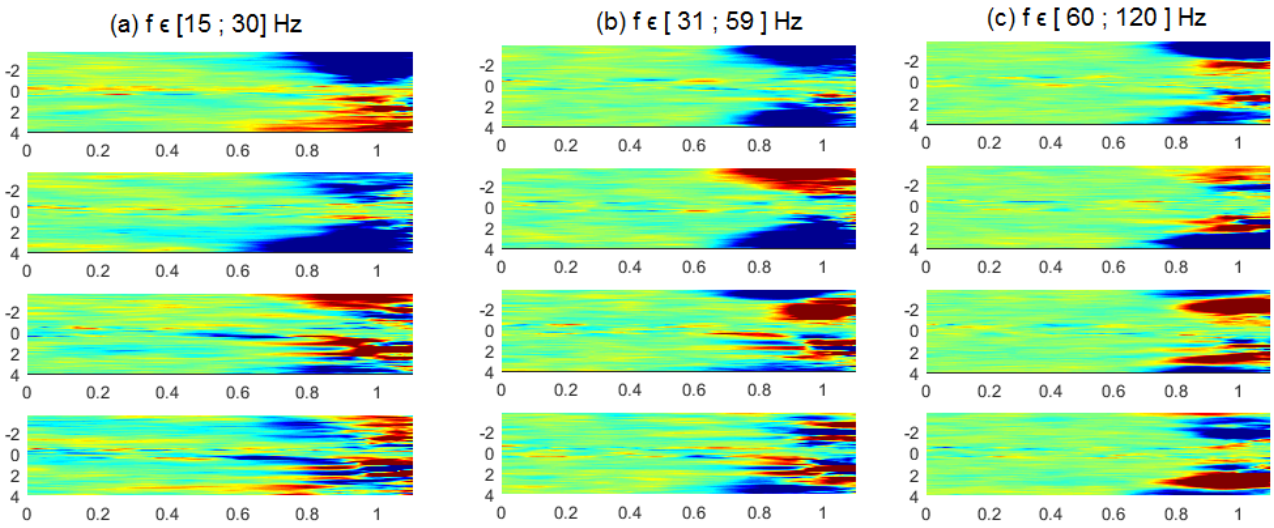

Figure 14 - Case 7; 1 jet ; $\frac{L}{d} = 1.1024$; $Re = 13{,}924$; Main modes observed for v'_{rms}

The frequency band [15 ; 30] Hz showed to concentrate the greatest portion of the modes energy, for all measured flows. It was deemed as the band that best represents the oscillatory phenomena for this type of annular flow.

The heat transfer analysis was initiated with the calculation of Nu_d, according to Eq. (2.2). Two examples of Nu_d distributions found are shown in Figure 15. The variable on the vertical axis, s is the curvilinear coordinate along the plate, given by $s = \theta \cdot R_{external}$. In all experiments, $R_{external} = 25\ mm$.

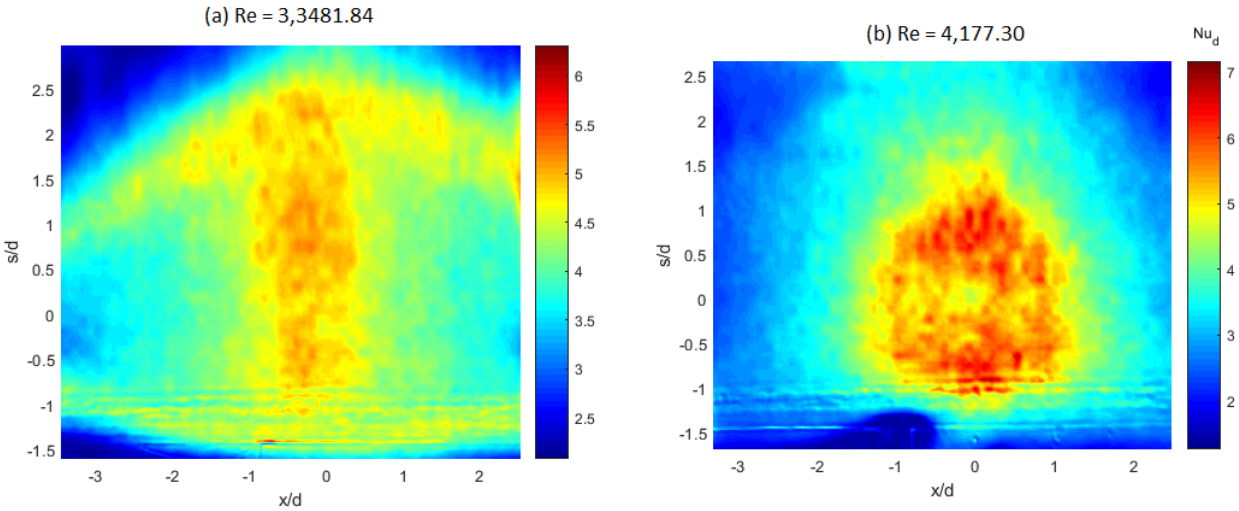

Figure 15 - Local Nu_d distributions, for 1 jet ; $\frac{L}{d} = 0.9449$

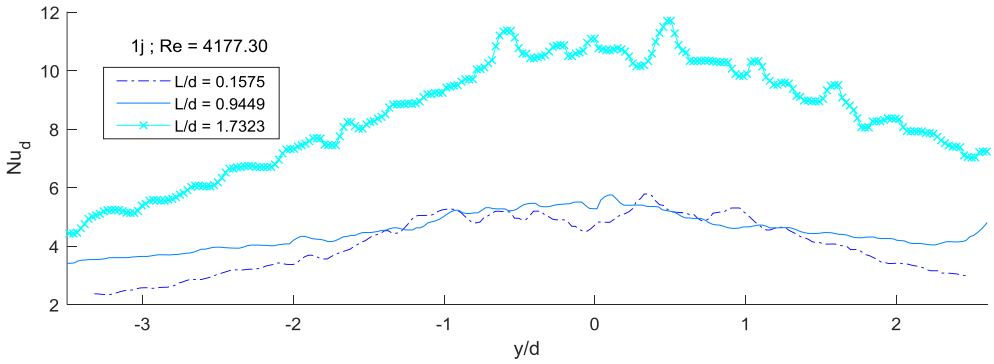

Figure 16 - Local Nu_d vs. y ; 1 jet ; $\frac{L}{d} = 0.9449$.

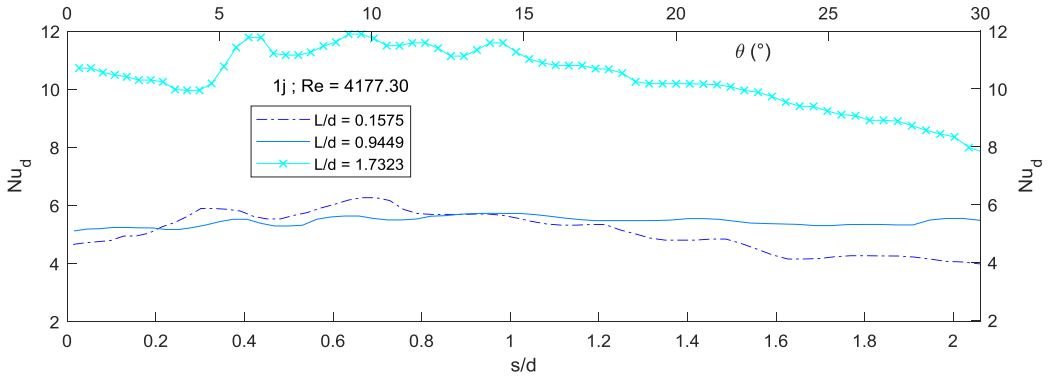

Figure 17 - Local Nu_d vs. θ ; 1 jet ; $\frac{L}{d} = 0.9449$.

The curve corresponding to $\frac{L}{d} = 1.7323$ is above the $\frac{L}{d} = 0.1575$ curve, in opposed to what one would normally expect. However, by analyzing the PIV data, this inversion was found to be possible and corroborated.

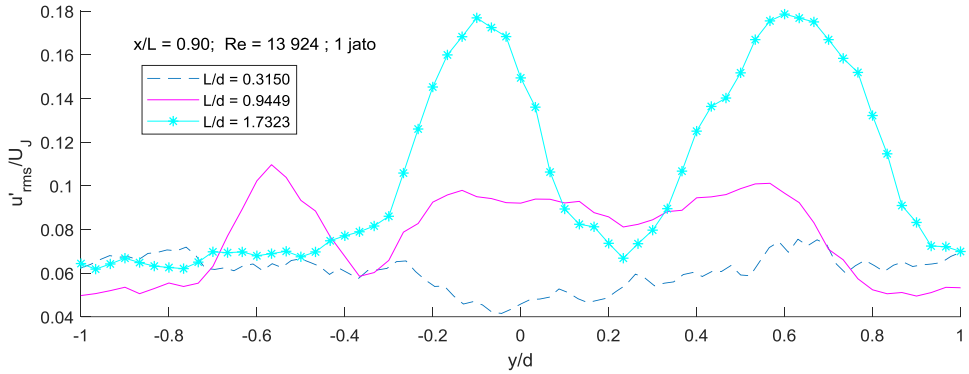

Figure 18 – Fluctuations in stremwise speed; 1 jet ; $Re = 13{,}924$

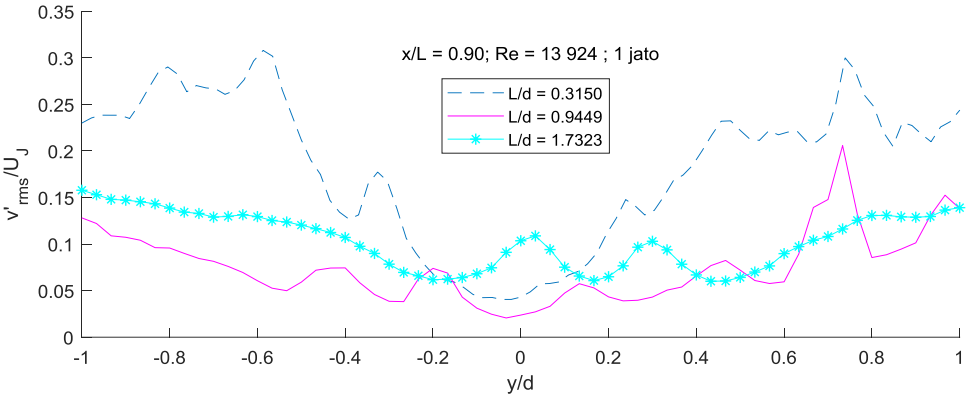

Figure 19 – Fluctuations in crosswise speed; 1 jet ; $Re = 13{,}924$

For comparison purposes, the experiment was repeated for other geometries.

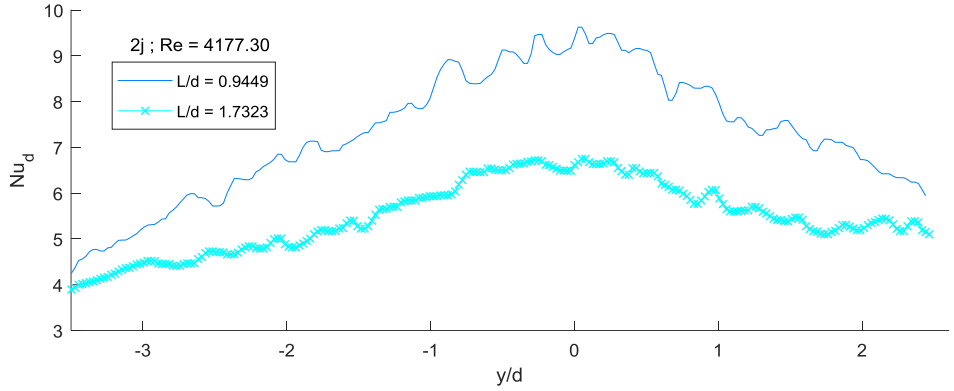

Figure 20 - Local Nu_d vs y ; 2 jets ; $Re = 4{,}177$

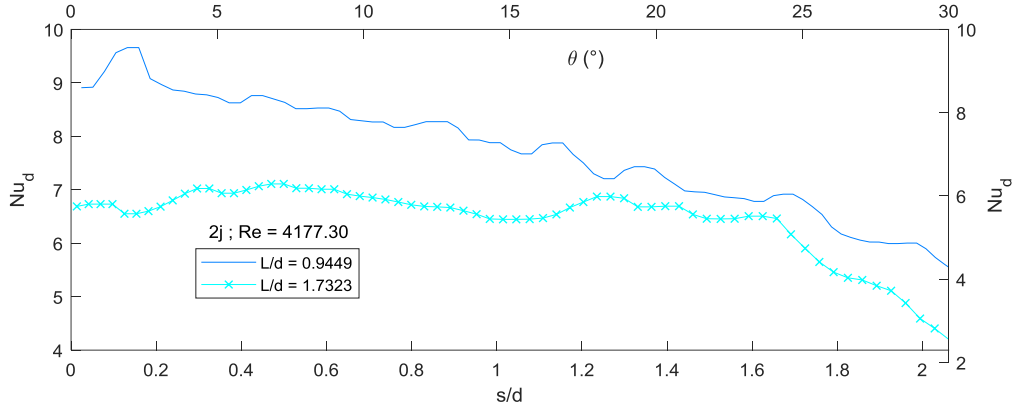

Figure 21 - Local Nu_d vs θ ; 2 jets ; $Re = 4{,}177$

For these geometries, the behavior of the Nu_d curves followed what was expected, with higher Nusselt values for the smaller gap. It wasn't possible to execute the experiment for 2 jets and $\frac{L}{d} = 0.1575$, due to limitations on pump pressure.

Finally, an analysis was carried out, to investigate the influence of the Reynolds number on Nu_d. For this experiment, the configuration with 2 jets and $\frac{L}{d} = 1.7323$ was elected.

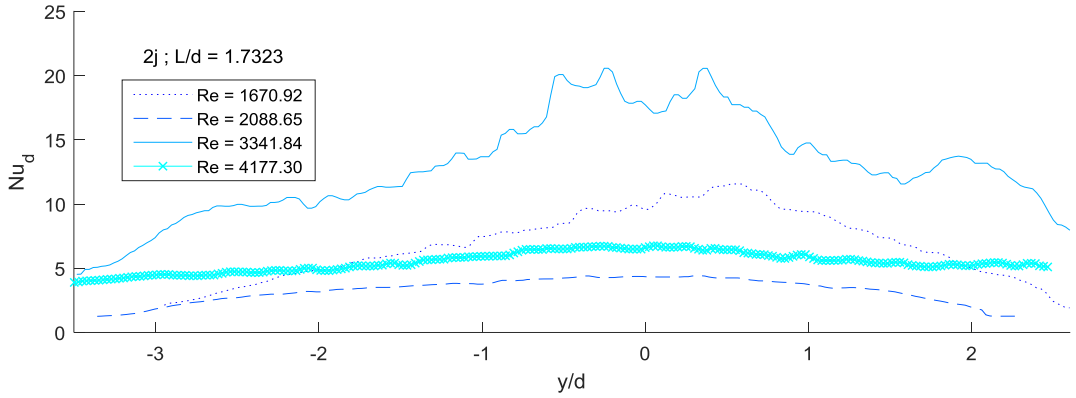

Figure 22 - Local Nu_d vs. y ; 2 jets ; $\frac{L}{d} = 1.7323$

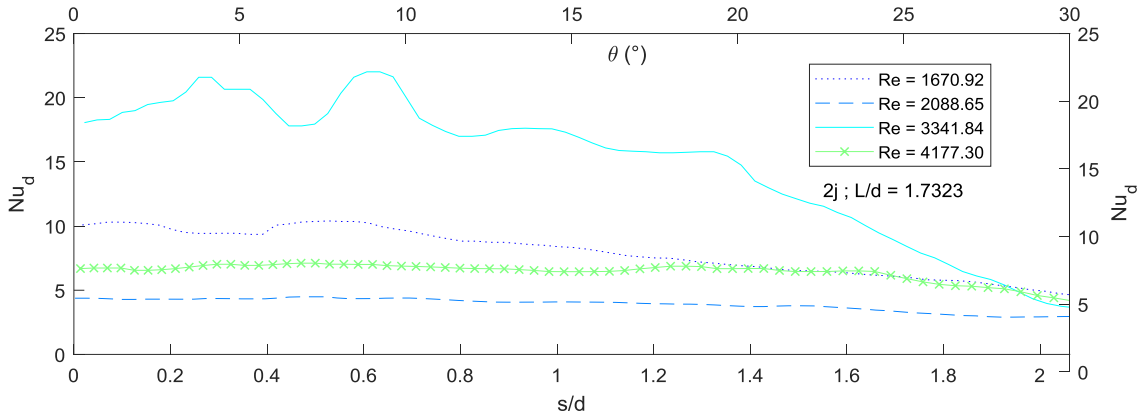

Figure 23 - Local Nu_d vs θ ; 2 jets ; $\frac{L}{d} = 1.7323$

A very peculiar behavior was observed, for the curves. There seems to be another parameter, besides Re, which is affecting the heat transfer rate. High Reynolds number, even though can bring more turbulence to the annular flow, can also make this turbulence less effective, under the heat transfer perspective. This could be happening due the occurrence of less coherent vortices, for some values of Reynolds rather than for others.

All Nu_d distributions was found to be in line with experiments performed throughout literature, such as Azimi (2015) and Kayansayan (2001).

4. CONCLUSIONS

The study allowed, for the first time, an investigation of the behavior of impinging jets in a confined cavity. The present of circulation within the annular space entangled the jet exiting from the nozzles, altering the velocity profiles that would be expected for a conventional impinging jet. Some other differences were found, such as the initial acceleration in streamwise velocity, followed by its decrease to zero, on the wall. High turbulence is still observed in the same area as non-confined impinging jets, within 1 to 2 diameters of distance to the stagnation point.

A series of dominant vortex were found between 15 and 30 Hz and a simplified model of the flow was successfully constructed, with POD.

For the heat transfer experiments, It was possible to observe the second peaks on the Nusselt number, in a consistent fashion, near $\theta \in [6° \ ; 7{,}5°]$ and $\frac{y}{d} \in [0{,}5 \ ; 0{,}6]$. These second peaks of Nu_d were noticed in great part of the measured cases, often surpassing the value of Nusselt at the stagnation point, Nu_{d0}.

5. REFERENCES

Abrantes, J.K., Braga, I.B., Azevedo, L.F.A., Medição de escoamentos turbulentos utilizando velocimetria por imagem de partículas, PUC-RIO, Departamento de Engenharia Mecânica.

Berkooz, G., Holmes, P., Lumley, J., The Proper Orthogonal Decomposition in the Analysis of Turbulent Flows, Annual Review of Fluid Mechanics 1993. 25 : 539-75

Choi, M., Han, S.Y., Yang, G., Lee, J.S., Sohn, D.K., 2000. Measurements of impinging jet flow and heat transfer on a semi-circular concave surface. Int. J. Heat Mass Transfer 43, 1811–1822.

Cornaro, C., Fleischer, A.S., Goldstein, R.J., 1999. Flow visualization of a round jet impinging on cylindrical surfaces. Exp. Therm. Fluid Sci.20, 66–78.

Hashiehbaf, A.et al. / International Journal of Heat and Fluid Flow 53 (2015) 167–182

Kayansayan, N., Küçüka, S., Impingement cooling of a semi-cylindrical concave channel by confined slot-air-jet, Experimental Thermal and Fluid Science 25 (2001) 383-396

Zuckerman, N., Lior, N., Jet Impingement Heat Transfer: Physics, Correlations, and Numerical Modeling, Advances in Heat Transfer vol. 39, 2006

Chauchat, N., Schall, E., Cooling of a heating cylinder by comfined impacting air jets, International Journal of Numerical Methods for Heat & Fluid Flow, Vol. 26 (2016), Issue: 7, pp.2013-2032

Gori, F., Bossi, L., On the cooling effect of an air jet along the surface of a cylinder, Int. Comm. Heat and Mass Transfer, Vol. 27 (2000), No. 5, pp. 667-676.

Nada, S.A., Slot/Slots air jet impinging cooling of a cylinder for different jets-cylinder configurations, Heat Mass Transfer (2006) 43: 135-148

6. RESPONSIBILITY NOTICE

The author is the only responsible for the printed material included in this paper.